

Article

Effect of Substituting CaO with BaO and CaO/Al₂O₃ Ratio on the Viscosity of CaO–BaO–Al₂O₃–CaF₂–Li₂O Mold Flux System

Zhirong Li, Xinchun You, Min Li, Qian Wang, Shengping He * and Qiangqiang Wang

College of Materials Science and Engineering, Chongqing University, Chongqing 400044, China; cqulzr@cqu.edu.cn (Z.L.); vanmeuen@cqu.edu.cn (X.Y.); sjzlimin@cqu.edu.cn (M.L.); q_wang@cqu.edu.cn (Q.W.); wtfwawj@163.com (Q.W.)

* Correspondence: heshp@cqu.edu.cn; Tel.: +86-023-6510-2469

Received: 20 December 2018; Accepted: 26 January 2019; Published: 28 January 2019



Abstract: The effect of substituting CaO with BaO and CaO/Al₂O₃ ratio on the viscosity of CaO–BaO–Al₂O₃–CaF₂–Li₂O mold flux system was studied by rotational viscosity method. The results showed that the viscosity increased with increasing BaO as a substitute for CaO, while the viscosity decreased with the increase in CaO/Al₂O₃ ratio. The viscous activation energy of the slags is from 92.1 kJ·mol^{−1} to 133.4 kJ·mol^{−1}. Either the Arrhenius or the Weymann–Frenkel equation can be applied to establish the viscosity prediction model. In this paper, the Weymann–Frenkel equation and a new optical basicity with regard to Al₂O₃ as an acidic oxide were applied to the modified NPL model for predicting the viscosity of CaO–BaO–Al₂O₃–CaF₂–Li₂O mold flux system. The estimated viscosity is in good agreement with the measured viscosity.

Keywords: viscosity; BaO; CaO/Al₂O₃ ratio; modified NPL model

1. Introduction

High Mn-high Al steel, exemplified by twin-induced plasticity (TWIP) steel, has high strength and good ductility, as well as a smaller density compared with plain steels due to high contents of aluminum and manganese. This perfectly accords with next-generation steel for automobiles, the development of which is continuously devoted to pursuing safety and energy conservation and environmental protection [1,2]. However, the high aluminum content, is an unprecedented challenge to the production of high Mn-high Al steel using continuous casting, and the key to the solution for this is to select a proper mold flux [3]. It is well known that high Al content in molten steel will react with the traditional CaO–SiO₂-based mold flux, leading to a sharp reduction of SiO₂ and an increase of Al₂O₃ in molten slags, as shown in Equation (1), which will convert the original CaO–SiO₂-based mold flux into CaO–Al₂O₃-based mold flux [4,5]. With a substantial change of components, the physical properties of the slag, such as melting temperature and viscosity, will change dramatically, deteriorating the lubrication and heat transfer of slags and further resulting in all kinds of casting defects and even casting interruption [6–10].



Significant efforts have been made to solve the casting problems by employing various kinds of mold fluxes. Strong oxidizing components, such as MnO and Fe₂O₃, which have priority over SiO₂ to react with Al in molten steel, have been added to mold fluxes so as to protect SiO₂ from oxidation [11],

but this still led to a big increase in Al_2O_3 and altered the performance of the mold fluxes. Naturally, the $\text{CaO-Al}_2\text{O}_3$ -based mold flux with low SiO_2 content was then introduced to cast high Mn-high Al steel in order to weaken or avoid interfacial reactions [7,12–14]. However, they still contain a small number of reactive components other than the low content of SiO_2 , such as B_2O_3 and Na_2O , as shown in Equations (2) and (3). The components of the $\text{CaO-BaO-Al}_2\text{O}_3\text{-CaF}_2\text{-Li}_2\text{O}$ mold flux system studied in this paper have been verified not to react with Al in molten steel from thermodynamic calculation at the temperature of steelmaking [15]. Thus, the mold flux system can essentially avoid the reactivity problem and possess good application prospects in the casting of high Mn-high Al steel.

Viscosity is one of the most important indexes for evaluating the performance of mold fluxes, as it has a significant effect on the lubrication of casting blanks. In industrial production, the viscosity of mold fluxes at 1300 °C (η) and casting speed (v) generally meet the correlation $\eta \cdot v = 1.0\text{--}3.5$ (Poise $\text{m} \cdot \text{min}^{-1}$), so as to meet the demands for adequate lubrication and heat transfer [16]. A significant amount of research regarding the effect of Al_2O_3 on the viscosity of different slag systems has been conducted [17–22], while little research has been reported on mold fluxes in the absence of SiO_2 . It has been concluded that Al_2O_3 exists as $[\text{AlO}_4]^{5-}$ ions with four coordinated oxygens and forms a tetrahedral network structure in basic melts [23,24]; however, more work needs to be done regarding how Al_2O_3 behaves in slags without SiO_2 . It was also found that substituting CaO with BaO can reduce the viscosity and improve the vitrification rate of mold fluxes [25], which are conducive to the lubrication of the casting blank in continuous casting process. Thus, the viscosity of the $\text{CaO-BaO-Al}_2\text{O}_3\text{-CaF}_2\text{-Li}_2\text{O}$ mold flux system with various BaO/CaO and CaO/ Al_2O_3 ratios in mass was studied in this paper.

Over the last few decades, a series of viscosity models has been developed to predict the viscosity of BF slags, refining slags and mold fluxes. The empirical and semi-empirical models, e.g., Urban model [26], Riboud model [27], Iida model [28,29] and NPL model [30], involve a numerical fit of viscosity to chemical composition based on Arrhenius or Weymann–Frenkel equation. A viscosity prediction model of the $\text{CaO-BaO-Al}_2\text{O}_3\text{-CaF}_2\text{-Li}_2\text{O}$ mold flux system according to the modified NPL model is established in this paper, and the estimated viscosity fits well with the experimental results.

2. Materials and Methods

2.1. Sample Preparation

Slag samples were prepared using reagent-grade Al_2O_3 , CaF_2 , CaO, BaCO_3 and Li_2CO_3 (Sinopharm Chemical Reagent Co., Ltd., Shanghai, China), with BaCO_3 and Li_2CO_3 being used as the sources for BaO and Li_2O , respectively. In a muffle furnace, Al_2O_3 , CaF_2 , BaCO_3 and Li_2CO_3 were calcined for 2 h at 500 °C to remove moisture, while CaO was calcined for 5 h at 1000 °C to decompose any carbonate and hydroxide before experiment. Table 1 gives the chemical compositions of samples. The prepared powders were then ground and weighed according to the designed compositions and mixed in a mortar for melting. Each fused sample was about 250 g.

Table 1. Chemical composition of experimental slags (wt %).

Slag No.	CaO	BaO	Al_2O_3	F^-	Li_2O	BaO/CaO	CaO/ Al_2O_3
S-1	36	14	34	8	8	0.39	-
S-2	32	18	34	8	8	0.56	-
S-3	28	22	34	8	8	0.79	-
S-4	24	26	34	8	8	1.08	0.71
S-5	28	26	30	8	8	-	0.93
S-6	32	26	26	8	8	-	1.23
S-vali ¹	24	30	30	8	8	1.25	0.80

¹ S-vali is a slag for validation of the modified NPL (National Physical Laboratory, Teddington, UK) model.

2.2. Viscosity Measurement

Viscosity was measured using a rotation viscometer. The experimental apparatus (Chongqing Safety Production Scientific Research Co., Ltd., Chongqing, China) for viscosity measurement is shown in Figure 1. A high-temperature furnace with U-shape MoSi₂ heating elements is monitored by a B-type thermocouple and a proportional-integral-derivative (PID) controller to ensure that the deviation of temperature in the uniform temperature zone can be maintained within ± 2 °C. Before the viscosity measurement, crucible and cylinder were set along the axis of the viscometer, and a calibration measurement was carried out at room temperature by using castor oil of known viscosity. Then, the furnace was heated to the experimental temperature (1400 °C) and held for 10 min to stabilize the temperature and homogenize the slag melt under an Ar gas atmosphere (flow rate: 0.5 L/min). After that the cylinder was carefully immersed into molten slag just 20mm above the bottom of graphite crucible and rotated at a speed of 12 rpm. When the signal from viscometer became stable, the furnace was cooled at a rate of 6 °C/min and the viscosity measurement started and lasted until the value of the measured viscosity reached nearly 3 Pa·S. In the end, the furnace was reheated to 1400 °C at a speed of 15 °C/min to pull out the cylinder and pour out the molten flux.

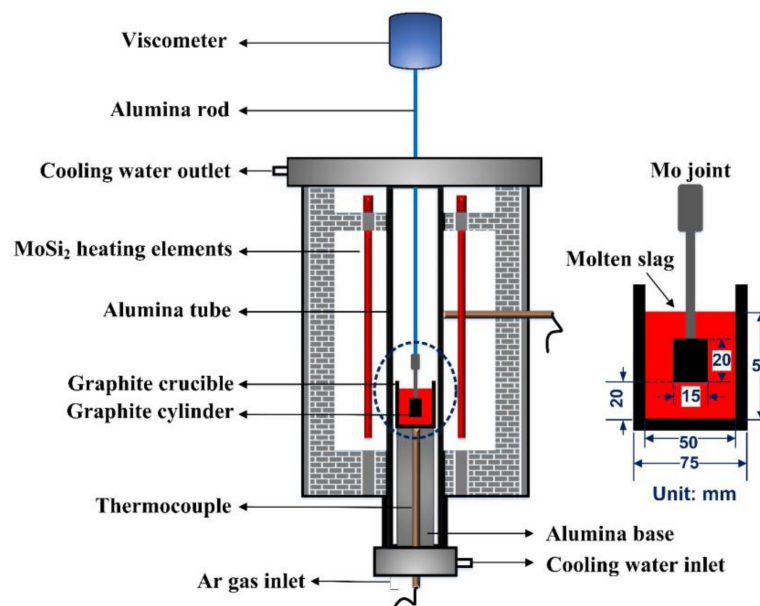


Figure 1. Schematic diagram for viscosity measurement.

3. Results and Discussion

3.1. The Effect of Substituting CaO with BaO on the Viscosity

Figure 2 shows the viscosity–temperature (η – T) curves of slags S-1 to S-4. Figure 3 shows the effect of substituting CaO with BaO on the viscosity of slags S-1 to S-4. It can be seen that the viscosity of the slags increases gradually with increasing BaO as a substitute for CaO. This is consistent with the trend observed by Wang et al. [31] for a CaO–BaO–SiO₂–MgO–Al₂O₃ slag system and Sukenaga et al. [32] for a CaO–SiO₂–Al₂O₃–BaO slag system (CaO/SiO₂ = 0.67 in mass). Meanwhile, it is inconsistent with the results observed for a BaO–CaO–Al₂O₃–MgO–B₂O₃–SiO₂–CaF₂–Li₂O slag system by Wu et al. [25], who found that the viscosity decreased with BaO substituting CaO. CaO and BaO, as alkaline-earth metallic oxides in the slags, have two completely different effects on the structure of the aluminates. On the one hand, as the Ba²⁺ ion radius (1.44 Å) is larger than the Ca²⁺ ion radius (1.08 Å) [33], the electrostatic potential of Ba²⁺ is smaller than that of Ca²⁺. That is, it is easier for BaO to dissociate free oxygen (O²⁻), and it possesses a greater depolymerization effect on network structure, which reduces the viscosity with BaO substituting CaO. On the other hand, in aluminosilicate systems, Al₂O₃

is a typical amphoteric oxide, and its behavior depends on the basicity of the melts [34]. When in an alkaline environment, it acts as a network former with charge compensation from cations and increases the complexity of the network structure. Since there is no SiO_2 in slags according to the composition in Table 1, Al_2O_3 serves as a network former and exists in the form of $[\text{AlO}_4]^{5-}$ tetrahedron with charge compensation from alkaline-earth metals [35]. As mentioned before, the electrostatic potential of Ba^{2+} is smaller than that of Ca^{2+} ; that is, the capacity of charge compensation of Ba^{2+} is stronger than that of Ca^{2+} ; therefore, substituting CaO with BaO can increase the structural stability of $[\text{AlO}_4]^{5-}$, which leads to the increase of the viscosity [31,36]. The experimental results indicate that the latter played a dominant role in affecting the network structure of the slags investigated in this study.

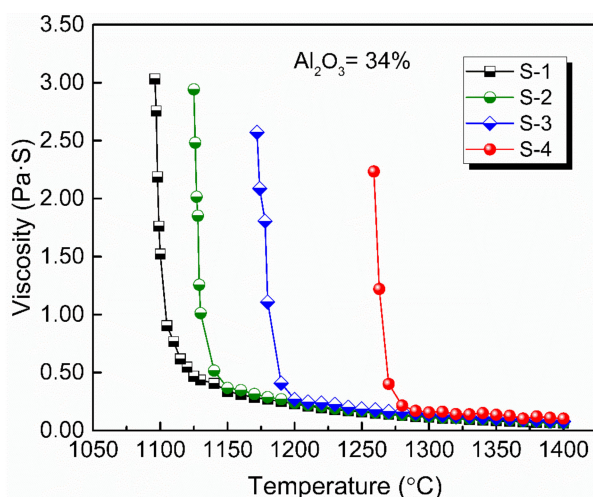


Figure 2. Viscosity–temperature curves of experimental slags with 34 wt % Al_2O_3 and various BaO/CaO ratios.

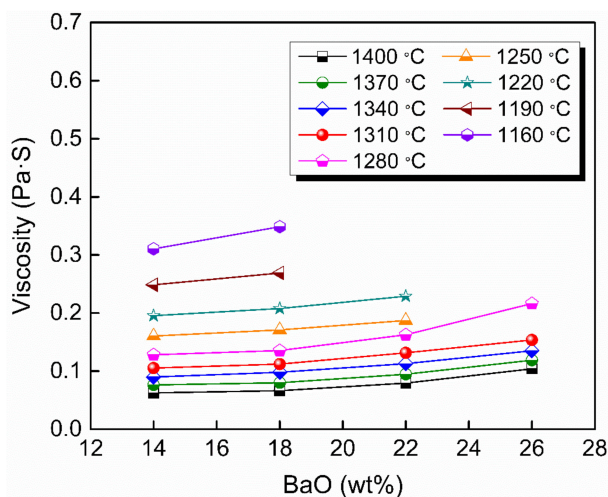


Figure 3. Viscosity of slags S-1 to S-4 in the fully fluid region with various BaO contents.

It should be noted that the substitution with BaO for CaO was performed by equal weight in mass. As the molecular weight of BaO is much greater than that of CaO , the free oxygen (O^{2-}) and charge compensation cations in the slags decreased after the substitution, which may also be a potential reason for the increase in viscosity.

3.2. Effect of $\text{CaO}/\text{Al}_2\text{O}_3$ Ratio on the Viscosity

Figure 4 shows the viscosity–temperature (η – T) curves of slags S-4 to S-6. Figure 5 shows the effect of $\text{CaO}/\text{Al}_2\text{O}_3$ ratio on the viscosity of slags S-4 to S-6. The results show that the viscosity of the slags decreased with the increase in $\text{CaO}/\text{Al}_2\text{O}_3$ ratio. This is consistent with the trend

observed by Behera et al. [22] for an $\text{Al}_2\text{O}_3\text{--Cr}_2\text{O}_3\text{--CaO--CaF}_2$ slag system and Xu et al. [37] for a $\text{CaO--Al}_2\text{O}_3\text{--MgO}$ slag system. Neuville et al. [38] studied the structure of crystals, glasses, and melts along $\text{CaO--Al}_2\text{O}_3$ join. The results show that Al is in octahedral coordination with high Al_2O_3 contents (>80 mol%) and essentially in fourfold coordination with 4 bridging O atoms (BOs) at Al_2O_3 contents of between 30 and 75 mol%. At around 25 mol% Al_2O_3 , Al is in tetrahedral coordination with two BOs. The presence of higher-coordinated species at high Al_2O_3 contents and their absence at low Al_2O_3 contents imply different viscous flow mechanisms for high- and low-concentration Al_2O_3 networks. That is, a higher $\text{CaO/Al}_2\text{O}_3$ ratio tends to increase the concentration of free oxygen (O^{2-}), leading to the depolymerization of $[\text{AlO}_4]^{5-}$ tetrahedron converting into simple structure units, reducing the complexity of the network structure and decreasing the viscosity [35]. Therefore, the viscosity decreased with the increase of $\text{CaO/Al}_2\text{O}_3$ ratio from slags S-4 to S-6.

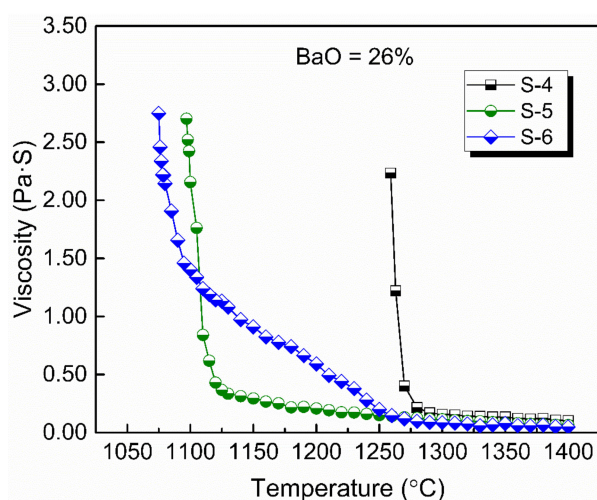


Figure 4. Viscosity–temperature curves of experimental slags with 26 wt % BaO and various $\text{CaO/Al}_2\text{O}_3$ ratios.

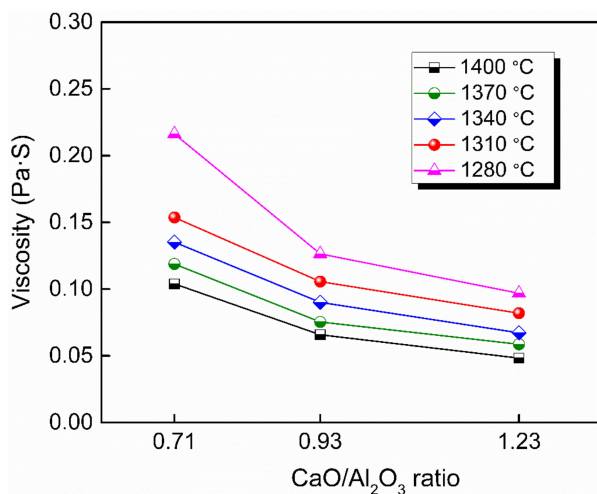


Figure 5. Viscosity of slags S-4 to S-6 in the fully fluid region with various $\text{CaO/Al}_2\text{O}_3$.

The optical basicity (Λ) can characterize the ‘availability’ of providing free oxygen ions, which indicates the degree of polymerization of the melts. A corrected optical basicity (Λ^{corr}) was proposed by Mills to charge balance the Al^{3+} ions incorporated into the Si^{4+} chain or ring [39]. Λ^{corr} is calculated by Equation (4), where X is the mole fraction, Λ is the optical basicity, and n refers to the number of oxygen atoms in the molecule, e.g., three for Al_2O_3 , and one for CaF_2 , etc., since two fluorine ions can be considered equivalent to one oxygen ion. A correction needs to be made in the calculation process: the component with the highest optical basicity will compensate the charge of Al_2O_3 first (if it is not

enough, the one with the second-highest optical basicity will continue to compensate, and so on), and the remaining, together with the components not participating in charge compensation, contributes to the corrected optical basicity of the slag system. The values of the corrected optical basicity (Λ^{corr}) of slags S-1 to S-6 are listed in Table 2. For a series of slags with a similar structure in the silicate system, the viscosity of slags generally decreases with the increase in basicity. This is also applied to slags S-4 to S-6, the viscosity of which decreases with the increase of the corrected optical basicity (Λ^{corr}). Similarly, the viscosity of slags increases with the decrease of corrected optical basicity (Λ^{corr}) for slags S-1 to S-4.

$$\Lambda^{\text{corr}} = \frac{\sum(X_1n_1\Lambda_1 + X_2n_2\Lambda_2 + X_3n_3\Lambda_3 \cdots)}{\sum(X_1n_1 + X_2n_2 + X_3n_3 \cdots)} \quad (4)$$

Moreover, Xu et al. found that the curves of viscosity versus CaO/Al₂O₃ ratio was a ‘V’ shape when studying the effect of CaO/Al₂O₃ ratio on the viscosity of a CaO–Al₂O₃–MgO slag system [37]. They deemed that the formation of low melting compounds (12CaO·7Al₂O₃) was conducive to the viscosity reduction. It can be seen from Table 2 that the variation tendency of the melting temperature is correspondingly in agreement with that of the viscosity for slags S-4 to S-6 or slags S-1 to S-4.

Table 2. Melting temperature (T_m), break temperature (T_{br}), corrected optical basicity (Λ^{corr}), new optical basicity (Λ_{new}), and viscous activation energy of experimental slags.

Slag No.	T_m (°C)	T_{br} (°C)	Λ^{corr}	Λ_{new}	E_η (kJ·mol ^{−1})	E_w (kJ·mol ^{−1})
S-1	1087	1132	0.760	1.760	133.4	146.2
S-2	1096	1148	0.753	1.771	131.0	143.9
S-3	1114	1196	0.748	1.783	119.1	132.2
S-4	1119	1285	0.743	1.797	91.2	101.3
S-5	1114	1124	0.777	1.787	118.1	130.9
S-6	1080	1268	0.811	1.778	121.9	135.3

3.3. Viscous Flow Activation Energy

It can be observed from the viscosity–temperature curves in Figures 2 and 4 that there is a temperature point below which the viscosity of the slag increases sharply in a narrow range of temperature. This temperature point is known as the break temperature (T_{br}), which can be obtained from the graph of the natural logarithm of viscosity versus inverse absolute temperature, as shown in Figure 6, taking slag S-3 as an example. When the temperature is above the T_{br} , the molten slag is in the state of fully liquid phase, and is a Newtonian fluid, while it presents as a non-Newtonian fluid when the temperature is below the T_{br} as a result of crystallization or solidification [40,41]. The break temperature of the slags is also listed in Table 2.

The temperature dependence of the viscosity is usually expressed by Arrhenius equation (Equation (5)) or Weymann–Frenkel equation (Equation (6)):

$$\eta = A \exp\left(\frac{E_\eta}{RT}\right), \quad (5)$$

$$\eta = AT \exp\left(\frac{E_w}{RT}\right), \quad (6)$$

where A is a proportionality constant, E_η and E_w are the activation energies for viscous flow, R is the gas constant and T is the absolute temperature. Figure 7 shows a linear relationship between $\ln\eta$ and $1/T$ and Figure 8 shows a linear relationship between $\ln(\eta/T)$ and $1/T$ in the Newton fluid region, from which the activation energy is obtained. The deviations between E_η and E_w for slags in the present study are below 10%, indicating that either the Arrhenius or Weymann–Frenkel equation can be used to evaluate the activation energy for viscous flow. The activation energies according to Arrhenius listed in Table 2 are from 91.2 kJ·mol^{−1} to 133.4 kJ·mol^{−1}, which are lower than those by Xu et al. [37] and Kim et al. [42], with their results being in the range of 175–400 kJ·mol^{−1}. It may be that the slags

in this study contained a higher content of fluxing agent—namely, Li_2O —and diluting agent—namely, CaF_2 . Additionally, the difference in network structure between their slags and the authors' slags also leads to a difference in activation energy.

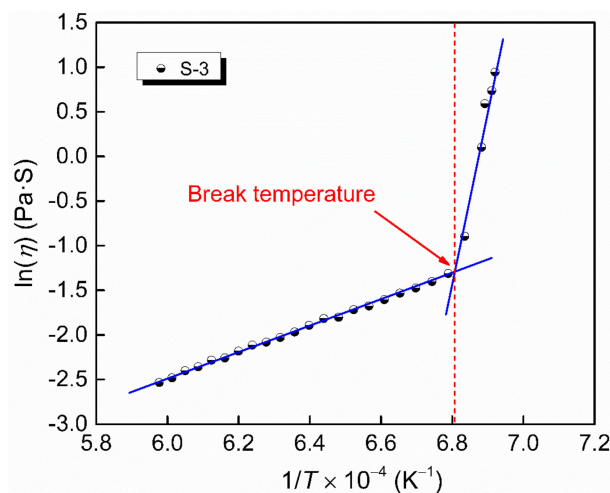


Figure 6. The natural logarithm of viscosity versus inverse absolute temperature of slag S-3.

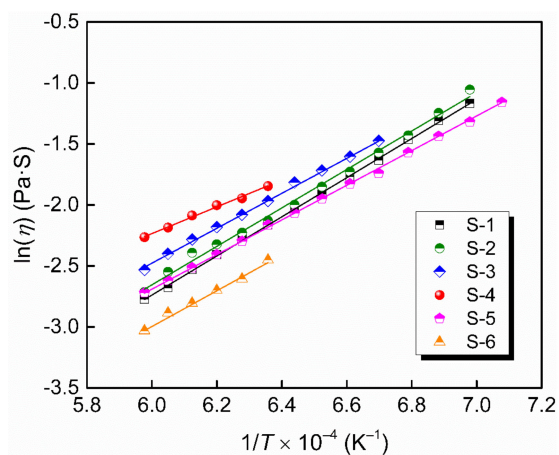


Figure 7. The natural logarithm of η as a function of $1/T$.

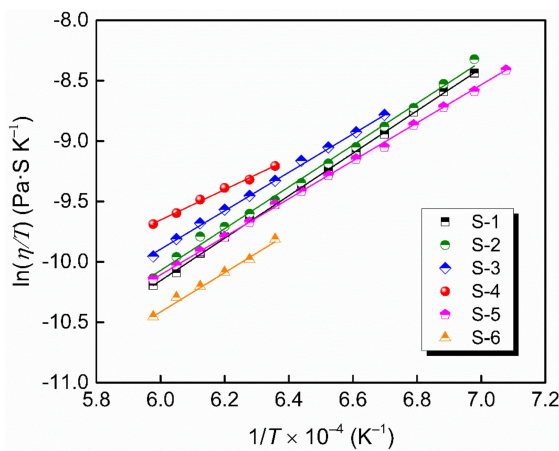


Figure 8. The natural logarithm of η/T as a function of $1/T$.

3.4. Industrial Application Prospect

To evaluate whether the viscosity of the slags in the present study is applicable for industrial application, 20Mn23AlV was selected as an instance. The casting speed of 20Mn23AlV is about 0.9 m/min, and the viscosities of the mold fluxes at 1300 °C in this paper are from 1.13 to 1.58 Poise; thus, the values of $\eta \cdot v$ are from 1.02 to 1.42, which meet the correlation $\eta \cdot v = 1.0\text{--}3.5$ ($\text{Poise} \cdot \text{m} \cdot \text{min}^{-1}$). Moreover, according to the above empirical formula, the fluxes studied in this paper can be applied to industrial production with a maximum casting speed of approximately 3 m/min. Meanwhile, the casting speed of high Mn-high Al steel in industrial production is generally less than 2 m/min, due to the solidification characteristics of the steels and the limitations of the actual casting conditions. Therefore, from the perspective of slag viscosity, the fluxes studied in this paper have good prospects for industrial application. Nevertheless, other properties, such as break temperature, vitrification rate, etc., need to be taken into consideration, so as to select a proper mold flux.

4. Viscosity Model

Since viscosity measurement is time-consuming work, several researchers have tried to establish various viscosity models to predict the viscosity of slags, e.g., the Riboud model [27,43], the Urbain model [26,44], the Iida model [28], the KTH model [45], and the NPL model [30,46,47]. These viscosity models were mainly based on CaO–SiO₂-based slags or CaO–SiO₂–Al₂O₃-based slags with low Al₂O₃ content. Figure 9 shows the estimated viscosity against measured viscosity of slags in this study with the Urbain model, Riboud model, and NPL model. It can be observed that there is a large deviation between the viscosity predicted by the Urbain model and the Riboud model and the measured viscosity. However, the predicted results according to the NPL model are much better, with some estimated viscosity being in good agreement with the measured viscosity, while the rest does not have a large deviation. Therefore, a modified NPL model based on the Weymann–Frenkel equation and optical basicity to predict the viscosity of slags was established in this study.

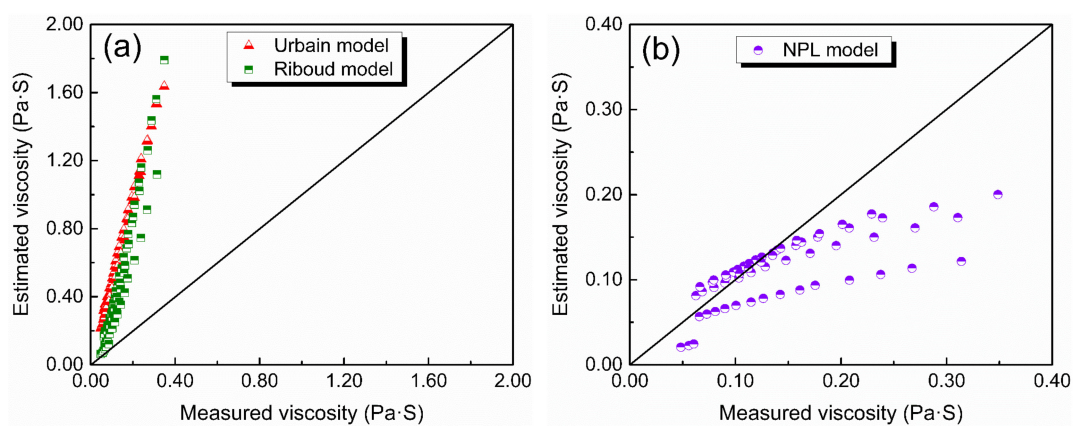


Figure 9. The estimated viscosity against the measured viscosity using different models: (a) Urbain and Riboud models, (b) NPL model.

The Weymann–Frenkel equation (Equation (6)) can be rewritten as follows:

$$\ln \frac{\eta}{T} = \ln A + \frac{1000B}{T}, \quad (7)$$

where parameter B ($B = \frac{E_w}{1000R}$) is a quadratic expression of the optical basicity, parameters A and B are in a linear relationship [44,46]. Moreover, according to the intercept and slope of each fitted line in Figure 8, the values of parameters A and B of each mold flux (or each optical basicity) can be obtained, respectively.

Similar to the traditional definition of basicity, Shankar et al. [47] redefined the optical basicity, termed as the new optical basicity, and its expression is as follows:

$$\Lambda_{\text{new}} = \frac{\frac{\sum (X_B n_B \Lambda_B + \dots)}{\sum (X_B n_B + \dots)}}{\frac{\sum (X_A n_A \Lambda_A + \dots)}{\sum (X_A n_A + \dots)}}. \quad (8)$$

In Equation (8), the new optical basicity is defined as the ratio of the total basic oxides to the total acidic oxides in the slag. Al_2O_3 is regarded as an acidic oxide in the slags studied in this paper, as it is the only network former of the molten slags. The new optical basicity is employed to predict the parameters A and B in Equation (7).

Figure 10 shows the relationship between the new optical basicity and parameter B calculated from the measured viscosity by Equation (7). Their relation can be fitted by a quadratic polynomial with a determination coefficient of 0.972, as shown in Equation (9). The parameters B and $\ln A$ are in a linear relationship, as shown in Figure 11, which can be expressed by Equation (10) with a determination coefficient of 0.981.

$$B = -4337.4\Lambda^2 + 15298.9\Lambda - 13473.2, \quad (9)$$

$$\ln A = -0.7057B - 8.3678. \quad (10)$$

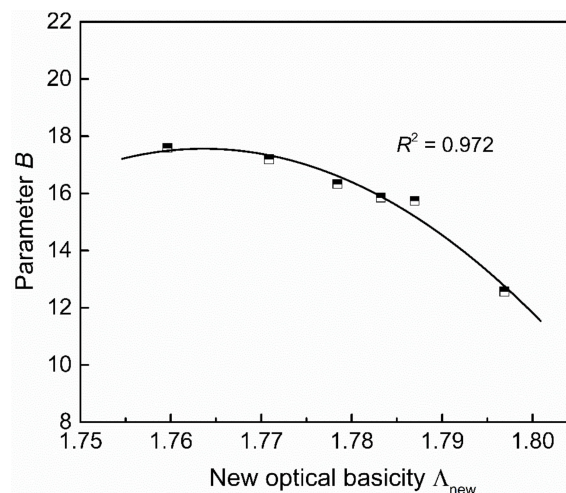


Figure 10. The relationship between the new optical basicity (Λ_{new}) and parameter B .

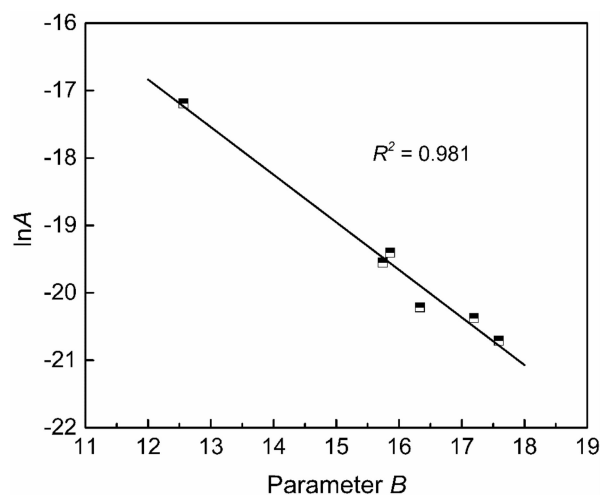


Figure 11. The relationship between parameters A and B .

Viscosity of the slags now can be calculated by Equations (7)–(10). The estimated viscosity compared with the measured viscosity is shown in Figure 12. It can be seen that the predicted viscosity by the modified NPL model is in a reasonable agreement with the experimental data with the deviation below 20%.

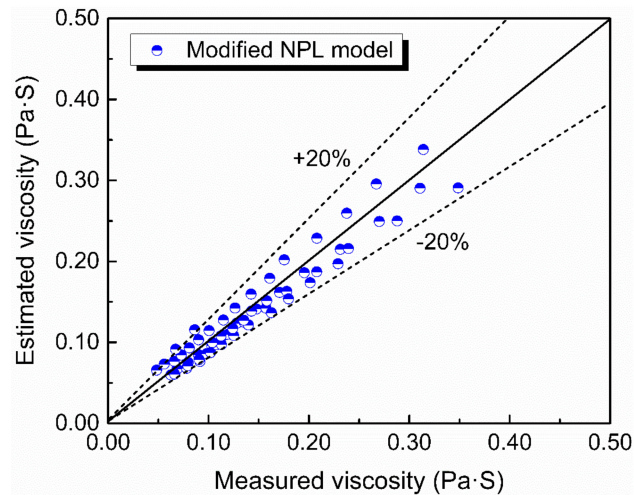


Figure 12. The estimated viscosity against the measured viscosity using modified NPL model.

To sum up, the modified parameters A and B , as well as a new optical basicity, were employed in the modified NPL model to reveal the dependence of viscosity on composition of CaO–Al₂O₃-based slag system in this study. As there is no measured viscosity data for slags with similar compositions in the other literature, an additional mold flux (S-vali) was measured with the composition listed in Table 1. Using the modified NPL model in this paper, it is found that the predicted and measured values also fit very well as shown in Figure 13.

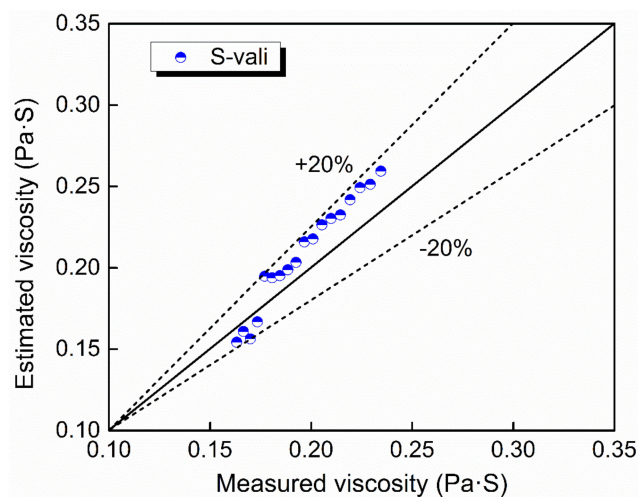


Figure 13. The estimated viscosity against the measured viscosity of S-vali using the modified NPL model.

5. Conclusions

In this paper, the effect of substituting CaO with BaO and CaO/Al₂O₃ ratio on the viscosity of CaO–BaO–Al₂O₃–CaF₂–Li₂O mold flux system was investigated. It was found that the viscosity of the slags increased with increasing BaO as a substitute for CaO, while the viscosity decreased with the increase of CaO/Al₂O₃ ratio due to the combination effect of depolymerization by free oxygen and polymerization by charge compensation on Al–O network structure. The deviation of the viscous activation energy calculated by Arrhenius and Weymann–Frenkel equations is less than 10%

and the values of the viscous activation energy according to Arrhenius equation are in the range of 92.1–133.4 kJ·mol⁻¹. The modified NPL model and the new optical basicity regarding Al₂O₃ as an acid oxide were employed to predict the viscosity. The prediction results show that the estimated viscosity is in a reasonable agreement with the measured value, with the deviation less than 20%.

Author Contributions: Z.L., S.H., Q.W. (Qian Wang), and Q.W. (Qiangqiang Wang) conceived and designed the experiment; Z.L., X.Y., and M.L. performed the experiment and analyzed the experimental data; Z.L. and Q.W. (Qiangqiang Wang) wrote the paper.

Funding: This research was funded by the Key Program of the National Natural Science Foundation of China (grant number U1660204) and the National Natural Science Foundation of China (grant numbers 51874057, 51804057) and the Fundamental Research Funds for the Central Universities in China (grant number 2018CDXYCL0018).

Conflicts of Interest: The authors declare no conflict of interest.

References

1. Neu, R. Performance and characterization of TWIP steels for automotive applications. *Mater. Perform. Charact.* **2013**, *2*, 244–284. [[CrossRef](#)]
2. Grässel, O.; Krüger, L.; Frommeyer, G.; Meyer, L. High strength Fe–Mn–(Al,Si) TRIP/TWIP steels development–properties–application. *Int. J. Plast.* **2000**, *16*, 1391–1409. [[CrossRef](#)]
3. He, S.; Li, Z.; Chen, Z.; Wu, T.; Wang, Q. Review of mold fluxes for continuous casting of high-alloy (Al,Mn,Ti) steels. *Steel Res. Int.* **2019**, *90*, 1800424. [[CrossRef](#)]
4. Fu, X.; Wen, G.; Liu, Q.; Tang, P.; Li, J.; Li, W. Development and evaluation of CaO–SiO₂ based mould fluxes for casting high aluminum TRIP steel. *Steel Res. Int.* **2015**, *86*, 110–120. [[CrossRef](#)]
5. Becker, J.J.; Madden, M.A.; Natarajan, T.T.; Piccone, T.; Serrano, E.; Story, S.; Ecklund-Baker, S.; Nickerson, I.; Schlichting, W. Liquid/Solid Interactions during Continuous Casting of High-Al Advanced High Strength Steels. In Proceedings of the AISTech-Conference, Charlotte, NC, USA, 9–12 May 2005.
6. Blazek, K.; Yin, H.; Skoczylas, G.; McClymonds, M.; Frazee, M. Evaluation of Lime-silica and Lime-alumina Mold Powders Developed for Casting High Aluminum TRIP Steel Grades. In Proceedings of the METEC InSteelCon 2011, Düsseldorf, Germany, 27 June–1 July 2011.
7. Street, S.; James, K.; Minor, N.; Roelant, A.; Tremp, J. Production of high-aluminum steel slabs. *Iron Steel Technol.* **2008**, *5*, 38–49.
8. Xiong, Y.; Wen, G.-H.; Ping, T.; Huan, W. Behavior of mold slag used for 20Mn23Al nonmagnetic steel during casting. *J. Iron Steel Res. Int.* **2011**, *18*, 20–25.
9. Wu, T.; He, S.; Zhu, L.; Wang, Q. Study on reaction performances and applications of mold flux for high-aluminum steel. *Mater. Trans.* **2016**, *57*, 58–63. [[CrossRef](#)]
10. Ji, C.; Yang, C.; Zhi, Z.; Tian, Z.; Zhao, C.; Zhu, G. Continuous casting of high-Al steel in Shougang Jingtang steel works. *J. Iron Steel Res. Int.* **2015**, *22*, 53–56. [[CrossRef](#)]
11. He, S.; Wang, Q.; Zeng, J.; Zhang, M.; Xie, B. Properties control of mold fluxes for high aluminum steel. *J. Iron Steel Res.* **2009**, *12*, 59–62.
12. Cho, J.; Blazek, K.; Frazee, M.; Yin, H.; Park, J.H.; Moon, S.W. Assessment of CaO–Al₂O₃ based mold flux system for high aluminum TRIP casting. *ISIJ Int.* **2013**, *53*, 62–70. [[CrossRef](#)]
13. Liu, Q.; Wen, G.; Li, J.; Fu, X.; Tang, P.; Li, W. Development of mould fluxes based on lime–alumina slag system for casting high aluminium TRIP steel. *Ironmak. Steelmak.* **2014**, *41*, 292–297. [[CrossRef](#)]
14. Yu, X.; Wen, G.; Tang, P.; Wang, H. Investigation on viscosity of mould fluxes during continuous casting of aluminium containing TRIP steels. *Ironmak. Steelmak.* **2009**, *36*, 623–630. [[CrossRef](#)]
15. Wu, T.; He, S.; Guo, Y.; Wang, Q. Study on reactivity between mould fluxes and high-Al molten steel. *Charact. Miner. Met. Mater.* **2014**, 265–270.
16. Nakano, T.; Kishi, T.; Koyama, K.; Komai, T.; Naitoh, S. Mold powder technology for continuous casting of aluminum-killed steel. *Trans. Iron Steel Inst. Jpn.* **1984**, *24*, 950–956. [[CrossRef](#)]
17. Zhang, Z.; Wen, G.; Tang, P.; Sridhar, S. The influence of Al₂O₃/SiO₂ ratio on the viscosity of mold fluxes. *ISIJ Int.* **2008**, *48*, 739–746. [[CrossRef](#)]
18. Xu, J.F.; Zeng, T.; Sheng, M.Q.; Jie, C.; Wan, K.; Zhang, J.Y. Viscosity of low silica CaO–5MgO–Al₂O₃–SiO₂ slags. *Ironmak. Steelmak.* **2014**, *41*, 486–492. [[CrossRef](#)]

19. Zhang, X.; Jiang, T.; Xue, X.; Hu, B. Influence of MgO/Al₂O₃ ratio on viscosity of blast furnace slag with high Al₂O₃ content. *Steel Res. Int.* **2016**, *87*, 87–94. [[CrossRef](#)]
20. Kim, G.H.; Sohn, I. Effect of Al₂O₃ on the viscosity and structure of calcium silicate-based melts containing Na₂O and CaF₂. *J. Non-Cryst. Solids* **2012**, *358*, 1530–1537. [[CrossRef](#)]
21. Li, J.; Shu, Q.; Chou, K. Effect of Al₂O₃/SiO₂ mass ratio on viscosity of CaO–Al₂O₃–SiO₂–CaF₂ slag. *Ironmak. Steelmak.* **2015**, *42*, 154–160. [[CrossRef](#)]
22. Behera, R.; Mohanty, U. Viscosity of Molten Al₂O₃–Cr₂O₃–CaO–CaF₂ Slags at Various Al₂O₃/CaO Ratios. *ISIJ Int.* **2001**, *41*, 834–843. [[CrossRef](#)]
23. Wu, T.; Wang, Q.; Yao, T.; He, S. Molecular dynamics simulations of the structural properties of Al₂O₃-based binary systems. *J. Non-Cryst. Solids* **2016**, *435*, 17–26. [[CrossRef](#)]
24. Kang, Y.; Morita, K. Thermal conductivity of the CaO–Al₂O₃–SiO₂ system. *ISIJ Int.* **2006**, *46*, 420–426. [[CrossRef](#)]
25. Wu, T.; Wang, Q.; He, S.; Xu, J.; Long, X.; Lu, Y. Study on properties of alumina-based mould fluxes for high-Al steel slab casting. *Steel Res. Int.* **2012**, *83*, 1194–1202. [[CrossRef](#)]
26. Urbain, G. Viscosity estimation of slags. *Steel Res.* **1987**, *58*, 111–116. [[CrossRef](#)]
27. Riboud, P.; Roux, Y.; Lucas, L.; Gaye, H. Improvement of continuous casting powders. *Fachberichte Huttenpraxis Metallweiterverarbeitung* **1981**, *19*, 859–869.
28. Iida, T.; Sakai, H.; Kita, Y.; Shigeno, K. An equation for accurate prediction of the viscosities of blast furnace type slags from chemical composition. *ISIJ Int.* **2000**, *40*, S110–S114. [[CrossRef](#)]
29. Iida, T.; Sakai, H.; Kita, Y.; Murakami, K. Equation for estimating viscosities of industrial mold fluxes. *High. Temp. Mater. Processes* **2000**, *19*, 153–164. [[CrossRef](#)]
30. Mills, K.; Sridhar, S. Viscosities of ironmaking and steelmaking slags. *Ironmak. Steelmak.* **1999**, *26*, 262–268. [[CrossRef](#)]
31. Wang, Z.; Sohn, I. Effect of substituting CaO with BaO on the viscosity and structure of CaO–BaO–SiO₂–MgO–Al₂O₃ slags. *J. Am. Ceram. Soc.* **2018**, *101*, 4285–4296. [[CrossRef](#)]
32. Sukenaga, S.; Saito, N.; Kawakami, K.; Nakashima, K. Viscosities of CaO–SiO₂–Al₂O₃–(R₂O or RO) melts. *ISIJ Int.* **2006**, *46*, 352–358. [[CrossRef](#)]
33. Whittaker, E.; Muntus, R. Ionic radii for use in geochemistry. *Geochim. Cosmochim. Acta* **1970**, *34*, 945–956. [[CrossRef](#)]
34. Kou, T.; Mizoguchi, K.; Sugino, Y. The Effect of Al₂O₃ on the Viscosity of Silicate Melts. *J. Jpn. Inst. Met.* **1978**, *42*, 775–781. [[CrossRef](#)]
35. Licheron, M.; Montouillout, V.; Millot, F.; Neuville, D.R. Raman and ²⁷Al NMR structure investigations of aluminate glasses: (1 – x)Al₂O₃ – xMO, with M = Ca, Sr, Ba and 0.5 < x < 0.75. *J. Non-Cryst. Solids* **2011**, *357*, 2796–2801.
36. Gao, E.; Wang, W.; Zhang, L. Effect of alkaline earth metal oxides on the viscosity and structure of the CaO–Al₂O₃ based mold flux for casting high-Al steels. *J. Non-Cryst. Solids* **2017**, *473*, 79–86. [[CrossRef](#)]
37. Xu, J.; Zhang, J.; Jie, C.; Ruan, F.; Chou, K. Experimental measurements and modelling of viscosity in CaO–Al₂O₃–MgO slag system. *Ironmak. Steelmak.* **2011**, *38*, 329–337. [[CrossRef](#)]
38. Neuville, D.R.; Henderson, G.S.; Cormier, L.; Massiot, D. The structure of crystals, glasses, and melts along the CaO–Al₂O₃ join: Results from Raman, Al L- and K-edge X-ray absorption, and ²⁷Al NMR spectroscopy. *Am. Mineral.* **2010**, *95*, 1580–1589. [[CrossRef](#)]
39. Mills, K.C. The influence of structure on the physico-chemical properties of slags. *ISIJ Int.* **1993**, *33*, 148–155. [[CrossRef](#)]
40. Brandaleze, E.; Di Gresia, G.; Santini, L.; Martín, A.; Benavidez, E. Mould Fluxes in the Steel Continuous Casting. In *Science and Technology of Casting Processes*; Srinivasan, M., Ed.; IntechOpen: London, UK, 2012; pp. 212–215.
41. Sridhar, S.; Mills, K.; Afrange, O.; Lörz, H.; Carli, R. Break temperatures of mould fluxes and their relevance to continuous casting. *Ironmak. Steelmak.* **2000**, *27*, 238–242. [[CrossRef](#)]
42. Kim, J.W.; Choi, J.; Kwon, O.H.; Lee, I.R.; Shin, Y.K.; Park, J.S. Viscous Characteristics of Synthetic Mold Powder for High Speed Continuous Casting. In *Proceedings of the 4th International Conference on Molten Slags and Fluxes*, Sendai, Japan, 8–11 June 1992.
43. Mills, K.; Yuan, L.; Jones, R. Estimating the physical properties of slags. *J. South. Afr. Inst. Min. Metall.* **2011**, *111*, 649–658.

44. Urbain, G.; Cambier, F.; Deletter, M.; Anseau, M.R. Viscosity of silicate melts. *Trans. J. Br. Ceram. Soc.* **1981**, *80*, 139–141.
45. Ji, F.Z.; Sichen, D.; Seetharaman, S. Experimental studies of the viscosities in the CaO–Fe_nO–SiO₂ slags. *Metall. Mater. Trans. B* **1997**, *28*, 827–834. [[CrossRef](#)]
46. Ray, H.; Pal, S. Simple method for theoretical estimation of viscosity of oxide melts using optical basicity. *Ironmak. Steelmak.* **2004**, *31*, 125–130. [[CrossRef](#)]
47. Shankar, A.; Görnerup, M.; Lahiri, A.; Seetharaman, S. Estimation of viscosity for blast furnace type slags. *Ironmak. Steelmak.* **2007**, *34*, 477–481. [[CrossRef](#)]



© 2019 by the authors. Licensee MDPI, Basel, Switzerland. This article is an open access article distributed under the terms and conditions of the Creative Commons Attribution (CC BY) license (<http://creativecommons.org/licenses/by/4.0/>).